Circular Economy 2 (2023) 100062

Contents lists available at ScienceDirect

Circular Economy

journal homepage: www.journals.elsevier.com/circular-economy

Original Research

Slag chemistry, element distribution behaviors, and metallurgical balance of e-waste smelting process

Fengchun Ye [a, b], Zhihong Liu [a], Longgong Xia [a, *]

[a] School of Metallurgy and Environment, Central South University, Changsha 410083, China
[b] China Nerin Engineering Co., Ltd, Nanchang, China

ARTICLE INFO

Article history:
Received 6 June 2023
Received in revised form
19 August 2023
Accepted 29 August 2023
Available online 21 November 2023

Keywords:
Circular economy
E-waste
Secondary copper
Dust
Recycling

ABSTRACT

The co-smelting of electronic waste (e-waste) in copper/lead pyrometallurgical processes is widely recognized as the preferred solution for sustainable development. However, aluminum and halogen elements in e-waste causes new challenges. To address this, the slag chemistry of high Al_2O_3-containing slag was studied, and the distribution behaviors of Au, Ag, Sn, and other elements in the copper alloy/slag/gas system were investigated in the presence of halogen elements (F/Cl/Br) using the equilibration method. The industrial practice of electronic waste smelting was modeled using METSIM, and the material and energy balances of one industrial process were obtained. Under the conditions of electronic waste smelting, the solubility of Al_2O_3 in the $FexO-SiO_2-Al_2O_3-CaO$ slag system decreased with increasing CaO content. When the CaO content was 20 wt%, and the Fe/SiO_2 mass ratio was 0.62–0.95, the solubility of Al_2O_3 in the slag reached 20 wt%. When 1%–10% CaF_2 was added, 93% of Au entered the metal phase. When the same amount of $CaCl_2$ or $CaBr_2$ was added, up to 32% Au entered the gas phase. When CaF_2 was added to the system, 22%–49% of Ag entered the gas phase. However, when $CaCl_2$ or $CaBr_2$ was added, 3%–34% of Ag entered the gas phase. The proportion of tin in the gas and slag phases increased with increasing temperature or the addition of halides. The METSIM simulation results showed that under optimized conditions, the crude copper contained more than 90 wt% copper, the discharged slag contained approximately 0.5 wt% copper, and the recovery rates of copper, gold, and silver were ≥98%. The heat generated from raw materials and fuel accounted for the largest part of the heat income, representing 65.32% of the total.

1. Introduction

Electronic waste (e-waste) mainly consists of waste circuit boards, printed circuit boards, copper-clad boards, their frame materials, and mixed electronic components. E-waste has become one of the fastest-growing solid wastes globally, with variable resources and potential pollutants, and has received widespread attention (Dwivedy & Mittal, 2010, 2012). China is the largest producer and consumer of electrical and electronic products globally, with the largest volume of electronic products available. According to the "2022 White Paper on the Recycling and Comprehensive Utilization of Waste Electrical and Electronic Products Industry", the theoretical amount of waste electrical and electronic products in China in 2021 is approximately 8.06 million tons (RCERGD, 2022).

According to the Association of Plastics Manufacturing in Europe, e-waste usually consists of 66% metals (38% of which are ferrous), 19% plastics, 4% glass, and 1% wood (Bazargan et al., 2012). Modern e-waste can contain 57 different elements (Kaya, 2016), some of which are precious metals; however, other elements are hazardous (Kuehr, 2019; Işıldar, 2018; Song et al., 2017). The metal content in e-waste can be 10 times larger than that in conventional minerals (Ahirwar & Tripathi, 2021) and this makes the recycling process quite profitable. On the other hand, the world's primary resources are currently depleted because of years of exploitation. However, global metal demand continues to increase exponentially every year. This exponential increase corresponds to the rapid development of current technologies, where the use of metal is still very much required in the manufacture of various technology hardwares (Kuehr, 2019), making the metal extracted from e-waste an alternative solution that is considered by many countries (Kaya, 2016). Developing green, efficient, and intensive technologies to treat waste electronic and electrical products, recycling valuable components

* Corresponding author.
E-mail address: longgong.xia@csu.edu.cn (L. Xia).

https://doi.org/10.1016/j.cec.2023.100062

(metal and nonmetal), and disposing of harmful elements are global concerns.

E-waste recycling can be accomplished through pyrometallurgical, hydrometallurgical, electrometallurgical, and biometallurgical processes (Ashiq, et al., 2019; Hoffmann, 1992; Sum, 1991).

The principle of the pyrometallurgical process is to smelt e-waste and obtain the molten metal phase and slag (Hoffmann, 1992). Typical pyrometallurgical processes of e-waste recycling in furnaces include incineration, combustion, pyrolysis, and molten phase formation. This method has the advantage of efficiently extracting valuable metals and treating hazardous substances. Currently, the most commonly used pyrometallurgical processes for recycling e-waste are copper smelter, lead smelter, or a combination of both. Pyrometallurgical routes are generally more economical, require less energy, and maximize precious metals (PMs) recovery. However, it has some limitations, such as large investment and the inability to recover organic components because they are used as a source of energy (Ebin & Isik, 2016; Hoffmann, 1992; Khaliq et al., 2014). Ceramic components in scrap increase the volume of slag, thereby increasing the loss of base metals and PMs. Fe and Al are not recovered as metals because they are oxidized into the slag phase (Ebin & Isik, 2016). It also generates hazardous emissions, particularly dioxins and halogenic compounds (Sum, 1991). In its application, the pyrometallurgical process is usually combined with a hydrometallurgical process to recover metals other than base metals, such as REE and PMs.

In the hydrometallurgical process, the main step consists of leaching solid materials with strong inorganic/organic acids or caustic watery solutions to selectively dissolve metals. The pregnant solutions were then subjected to separation and purification procedures (Tunsu & Retegan, 2016). To enrich these valuable metals, several steps are used, such as impurity precipitation, solvent extraction, adsorption, and ion exchange (Innocenzi, et al., 2017). The full hydrometallurgical process of e-waste exists as a mobile plant, but it has not been implemented on an industrial scale (Tunsu & Retegan, 2016). This process can be used to recover PMs during the recycling process. PMs from e-waste have been recovered successfully using hydrometallurgical technology. However, this technique has several disadvantages that prevent it from being used on a large scale. E-waste should be crushed into small pieces before leaching, which makes the process time-consuming and expensive. Another disadvantage is that toxic reagents are needed in this process, such as cyanide.

Combined technologies have also been used to separate valuable metals from e-waste, and these processes usually have pyrometallurgical unites, hydrometallurgical unites, and electrometallurgical unites (DOWA ECO-SYSTEM Co., Ltd., 2020; Hagelüken, 2006a, 2006b). The smelted metal forms an impure metal anode, which is then refined through electrorefining, in which the anode dissolves and deposits pure metal on the cathode. The electrometallurgical process is also used to obtain the metals contained in the pregnant solution from the hydrometallurgical process. These metals from leaching can be electrodeposited directly from the pregnant solution onto an inert cathode.

Owing to environmental issues generated using conventional metal recovery processes, an alternative eco-friendly method is being developed (Işıldar, 2018). Biometallurgy is a metal recovery method based on the microbial ability to use organic and inorganic substrates (Ashiq, et al., 2019). Microorganisms commonly used include bacteria, archaea, and fungi (Işıldar, 2018). Microorganisms are chosen for their ability to oxidize/utilize inorganic and organic substrates, resulting in lixiviant for metal dissolution. The use of microbial processes for the recovery of rare earth elements from e-waste could be hugely beneficial to many countries globally. Currently, bioleaching is being developed and considered as one of the most promising technologies for recovering metals from secondary resources because of its environmental performance and low cost.

Pyrometallurgy is the core step of treating e-waste based on the principles of “reduction, resource utilization, and harmless”, and it is the most promising technology in this field. However, the smelting of high aluminum, organic, and halogen-containing raw materials can easily lead to new problems, such as deterioration of slag performance, dispersion of valuable metals, and generation of dioxin pollutants. The mechanism of e-waste smelting is studied using theoretical analysis, principal experiments, and industrialization platform tests, which provide basic support for the research and development of e-waste utilization. The industrialization level of secondary material treatment can also be improved.

2. Methods

2.1. Phase equilibrium study

The equilibrium experiments were performed in a vertical tube furnace (KSL-1700X, Hefei Kejing Material Technology Co., Ltd.) under the electrical resistance of silicon carbide heating elements. The uniform temperature hot zone of the furnace was first confirmed by measuring its thermal profiles at various temperatures ranging from 800 °C to 1400 °C. The temperature of the hot zone was determined by using a calibrated S-type thermocouple. Special attention was paid to the accuracy of the equilibrium temperature, which was estimated to be ±2 °C for the entire experimental temperature range of interest. The specimen was kept in the hot zone at the target temperature for the required equilibration period. Special attention was paid to ensuring equilibrium by approaching the final equilibrium compositions with variations in the equilibration time. The equilibrium was determined by measuring the composition of the samples equilibrated at different times. To confirm the equilibrium, the equilibration experiments were repeated using both pure oxide powders and a single-phase solid solution. Three dedicated sets of experiments were performed to determine the equilibrium time. A longer equilibrium time is a positive factor in approaching the real equilibrium. Once the equilibrium time was reached, a bottle of water and ice mixture was attached to the bottom of the tube, and the specimen was rapidly quenched by dropping it into the ice-cold water bath. Subsequently, it was dried and mounted in epoxy resin. A polished cross-section of the mounted specimen was prepared using a conventional metallographic grinding and polishing technique.

2.2. Element distribution behaviors

The Fe_xO—SiO_2—CaO—Al_2O_3 system slag was synthesized by melting a well-mixed mixture of Fe_3O_4, SiO_2, CaO, and Al_2O_3 powders in a Pt crucible at 1350 °C for 8 h, and purified Ar gas (Hunan SaiZhong Gas Co., Ltd, purity 99.999 wt%) was used as the protective gas. In the experiment, 5 g of slag, 1 g of alloy, and a certain amount of calcium halides (CaF_2/$CaCl_2$/$CaBr_2$) were weighed and loaded into an Al_2O_3 crucible. The amount of halogen addition was set at 1%, 5%, and 10%, on the basis of alloy weight. Then, a notched corundum plate of appropriate size was placed above the reagent mixture, and another corundum crucible of the same size was assembled to the previously loaded crucible through a corundum sealant (supplied by Sinopharm Chemical Reagent Co., Ltd) to form a sealing system. The volatile products generated in the system were transmitted into the upper crucible and deposited on the inner surface of the notched plate.

The assembled sample was equilibrated at three different temperatures (1200 °C, 1300 °C, and 1400 °C) in a chamber furnace

(KSL-1400X, Hefei Kejing Material Technology Co., Ltd.). All visible metal droplets and particles were collected and weighed. After chemical digestion, the alloy samples were sent for inductively coupled plasma–mass spectrometry (ICP–MS) analysis. The influence of annealing temperature and halide addition dosage was studied. All experiments were labeled in the form of "kXm," where "k" refers to the information of equilibration temperature, and 12, 13, and 14 were used to represent 1200 °C, 1300 °C, and 1400 °C, respectively, "X" refers to the species of the halogen element, which can be F, Cl, and Br, and "m" refers to the adding dosage of halides, which can be 0, 1, 5, and 10. For example, "13Br5" refers to the sample equilibrated at 1300 °C and 5 wt% Br (based on alloy weight) was added in the experiment.

2.3. Metallurgical evaluation of the process

Material balance and heat balance (MB and HB) are critical characteristics of industrial practices that help evaluate material consumption, metal recoveries, and energy consumption. In this study, the MB and HB of one pilot e-waste smelting process were modeled using METSIM software. The NRT smelting process was used as the data source.

2.4. Analysis

Slag samples were mounted in epoxy resin, and a cross-section of the sample was prepared using a conventional metallographic grinding and polishing technique. After carbon coating, samples were analyzed using scanning electron microscopy (Tescan, Brno, Czech Republic) and energy-dispersive X-ray spectroscopy (Thermo Fisher Scientific, Waltham, Ma, USA) and further analyzed using electron microprobe analysis (EPMA) (JXA-8530, JEOL, Japan). The working parameters of EPMA used in this study were as follows, accelerating voltage 15 kV, working current 20 nA, and spot sizes of 5–30 μm. The standards used for different elements were, Fe (metallic Fe), Si (quartz, SiO_2), Ca (lime, CaO), Al (corundum, Al_2O_3), O (corundum, Al_2O_3), Cu (metallic Cu), Au (metallic Au), Ag (metallic Ag), Sn (metallic Sn), F (fluorite, CaF_2), Cl (antarcticite, $CaCl_2$), and Br (potassium bromide, KBr). For each phase in every sample, 5–10 spots were analyzed, and the data obtained were corrected using the Proza–Matrix program. The overall detection limit of EPMA was 0.01 wt%. The alloy sample was digested with aqua regia, and the Cu, Au, Ag, and Sn contents were analyzed using a plasma emission spectrometer (ICP-5100-VDV, Agilent Technologies, USA). The wavelengths used were Cu (324.75 nm), Au (242.80 nm), Ag (328.07 nm), and Sn (189.98 nm).

3. Results and discussion

3.1. Phase equilibrium of the Fe_xO–SiO_2–CaO–Al_2O_3 system

Iron can be Fe(II) or Fe(III) in the slag phase; therefore, this study focused on the Fe content and Fe/SiO_2 mass ratio in the slag phase. The influence of various parameters on the slag composition was studied by accounting for these data from equilibration experiments based on the calculated slag composition ($25\% \leq SiO_2 \leq 35\%$, $T_{Fe} \geq 15.5\%$, $CaO \geq 15\%$).

Fig. 1 shows that the magnetite content of the slag is an important factor that affects the copper content in the slag, and they have a positive relationship. Copper in the slag is approximately 1.3 wt%.

Fig. 2 shows that the Fe content is between 19.5% and 24%, and within this range, the relationship between the Fe content and the copper content in the slag is not obvious. However, when the Fe content is between 19.5% and 24%, it is not the major factor affecting the copper content in the slag. The Fe content between 19.5% and 24% is reasonable.

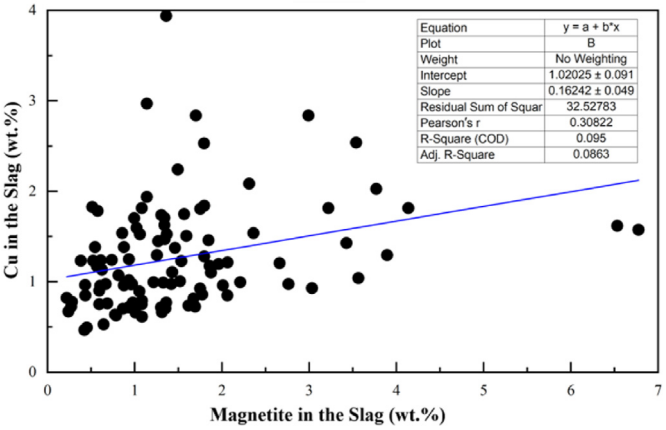

Fig. 1. Relationship between the copper loss in slag and magnetite content in slag.

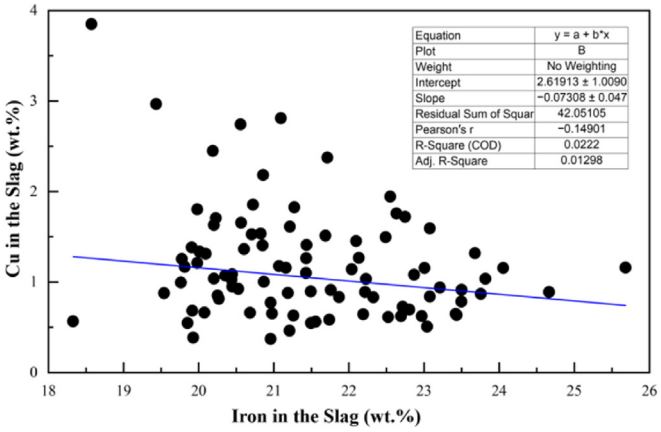

Fig. 2. Relationship between copper loss in slag and iron content in slag.

Fig. 3 shows that the Fe/SiO_2 mass ratio is 0.55–0.95, and within this range, the relationship between Fe/SiO_2 and the copper content in the slag is not obvious. Overall, there is a positive relationship between Fe/SiO_2 and the copper content in the slag. There was more copper in the slag, but it was still below 0.8%, and it decreased as the Fe/SiO_2 mass ratio of the slag increased.

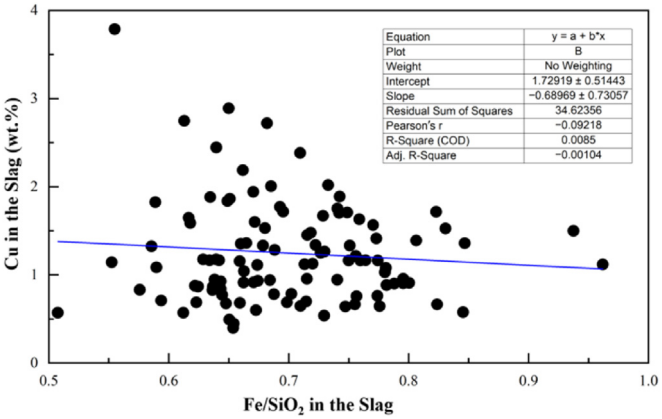

Fig. 3. Relationship between copper loss in slag and Fe/SiO_2 mass ratio of slag.

Fig. 4 shows that when the SiO_2 content is 28 wt%–35 wt%, the overall trend of the SiO_2 content decreases, whereas the overall trend of the copper content in the slag increases. The SiO_2 and copper contents in the slag are inversely related. There was a high distribution of slag with copper content below 0.8%, and it was more reasonable to control the SiO_2 content between 30 wt% and 35 wt%.

Fig. 5 shows that the slag has a copper loss below 0.8 wt%, indicating a reverse relationship between the CaO and slag copper contents. The amplitude of the CaO content change is relatively small, with most of the CaO content ranging from 19 wt% to 22 wt%, and the copper loss in the slag is higher than 1 wt%. In summary, the CaO content ranges from 22 wt% to 26.5 wt%, which is beneficial for reducing the copper content in the slag.

Fig. 6 shows the Al_2O_3 content at 11 wt%–19 wt%. The copper content in the slag was more sensitive to changes in the Al_2O_3 content, and there is a positive relationship between the Al_2O_3 and copper contents in the slag. Reduced Al_2O_3 content is beneficial for reducing copper content in the slag. The Al_2O_3 content in the slag was optimized to be less than 12 wt%.

Under fixed oxygen partial pressures, the FeO–SiO_2–Al_2O_3–CaO system can undergo slag-making reactions at low temperatures (Table 1). At the same temperature, the solubility of Al_2O_3 in the system decreases as the CaO content in the slag increases. When the CaO content was 20 wt% and the Fe/SiO_2 mass ratio was 0.62–0.95, the above slag system yielded a large Al_2O_3 dissolution. In the FeO–SiO_2–Al_2O_3–CaO system, the Fe_3O_4 content was generally high. The slag-making temperature of the system decreases within a certain range with the addition of CaO; however, when more CaO was added, a significant decrease in Al_2O_3 dissolution occurred.

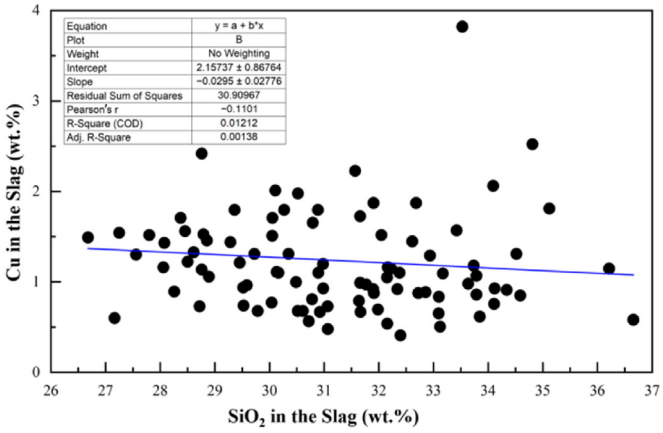

Fig. 4. Relationship between copper loss in slag and SiO_2 content in slag.

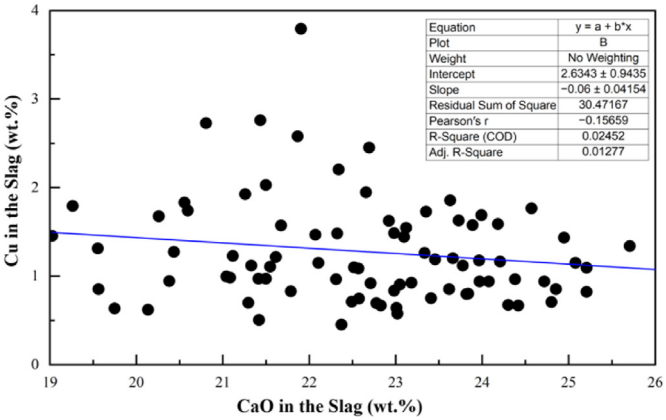

Fig. 5. Relationship between copper in slag and CaO content in slag.

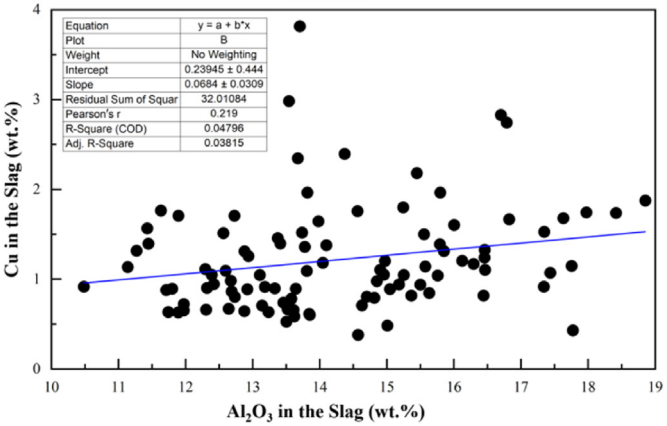

Fig. 6. Relationship between the copper in slag and Al_2O_3 content in the slag.

3.2. Distribution behavior of valuable metals

The presence of halogen elements influences the smelting behavior of valuable metals. The decomposition and burning of organic parts can produce halogen-containing gases. When running these experiments on a laboratory scale, the gases vented rapidly from the system. To understand the mechanism of dust formation, solid $CaCl_2$, CaF_2, and $CaBr_2$ chemicals were used as starting materials. The effects of the F content and temperature on the distribution behavior of Au, Ag, and Sn were experimentally studied. Based on the ICP results of the alloy phase and the EPMA results of the slag phase, the distribution behavior of Au, Ag, and Sn among the alloy, slag, and gas phases was statistically analyzed, and the obtained results are shown in Fig. 7.

Fig. 7 shows that when the halogen content in the system is zero, gold is mainly enriched in the alloy phase, and only trace amounts of gold can be detected in the slag. The gold content in the slag increased as the temperature increased. Silver has a distribution behavior similar to that of gold, with most silver enriched in the alloy phase and only a small amount entering the flue gas and slag phases. When the temperature increased, the silver content in the slag increased, whereas the silver content in the alloy phase first decreased and then increased. Tin was easily oxidized and mainly dissolved in the slag, whereas a small amount of tin was distributed in the gas and alloy phases. As the temperature increases, the dissolution of tin in the slag intensifies. After adding F to the system, some Au entered the gas phase, whereas the Au content in the slag slightly increased, and that in the alloy phase decreased. Although adding a certain amount of F could reduce the melting point and viscosity of the slag, which is conducive to the sedimentation of the alloy phase, it will decrease the direct yield of Au. As the F content in the system increased, the Ag content in the flue gas phase significantly increased, whereas the Ag content in the slag decreased, which could be due to the formation and volatilization of AgF. The addition of F to the system increased the content of Sn in the flue gas while decreasing the content distributed to the alloy and slag phases. In addition, temperature changes significantly affected the distribution behavior of gold, silver, and tin. As the F content in the system increases from 1200 °C to 1300 °C, the gold content in the alloy phase decreases. However, when the F content increased at

Table 1
The slag composition (wt%) of the FeO–SiO_2–Al_2O_3–CaO system at different temperatures.

Temperature (°C)	FeO	Fe_3O_4	Al_2O_3	SiO_2	CaO	Fe/SiO_2	CaO/Fe	CaO/SiO_2
1200	40–50	—	15–20	35–42	0	~0.88	0.00	0.00
1200	28–32	—	14–19	41–46	5	~0.55	~0.20	~0.11
1200	40–50	—	13–18	27–32	10	~1.17	~0.29	~0.33
1200	30–33	—	16–20	25–30	20	~0.86	~0.80	~0.69
1200	25–31	—	7–10	31–35	30	~0.68	~1.33	~0.91
1400	—	50–60	16–22	25–30	0	~1.58	0.00	0.00
1350	—	57–62	14–19	21–24	5	~2.02	~0.11	~0.23
1300	—	63–67	15–20	4–10	10	~7.22	~0.20	~1.43
1260	—	28–35	24–29	18–20	20	~1.35	~0.78	~1.05
1200	—	33–38	6–8	25–28	30	~1.04	~1.07	~1.11

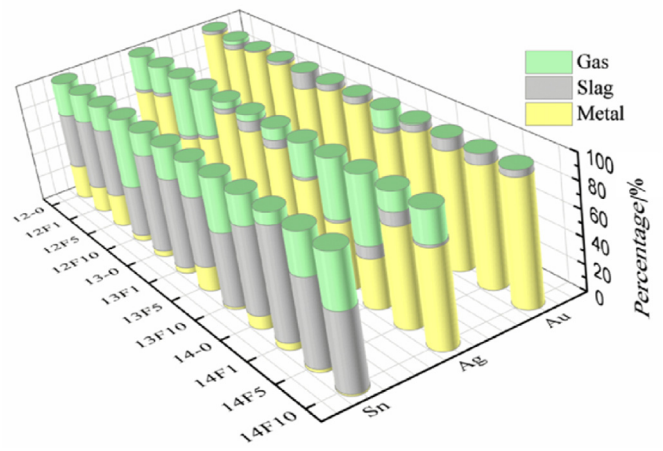

Fig. 7. Distribution behaviors of Au, Ag, and Sn in CaF_2 adding system.

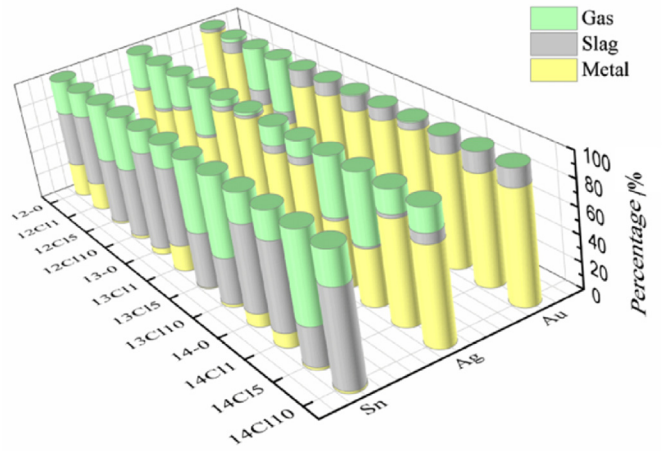

Fig. 8. Distribution behaviors of Au, Ag, and Sn in $CaCl_2$ adding system.

1400 °C, the Au content in the slag phase decreased. When an equal amount of F was added, the Sn content in the slag and flue gas increased with increasing temperature. Conversely, the effect of temperature on silver distribution behavior was relatively complex. When the F content in the system was 1 wt%, the Ag content in the flue gas and slag phases increased with increasing temperature. When the F content in the system was 5 or 10 wt%, the distribution ratio of Ag in the alloy phase increased, whereas the Ag content in the flue gas decreased. In summary, when the system temperature was constant, as the F content in the system increased, gold, silver, and tin were more easily distributed in the slag and flue gas phases, whereas the content in the alloy phase decreased, thereby decreasing the yield.

Fig. 8 shows that when Cl was added, Au, Ag, and Sn were distributed in the alloy, slag, and flue gas phases, respectively. When the temperature was 1200 °C, the distribution ratio of gold and silver in the flue gas increased sharply with increasing Cl content in the system, reaching a maximum of 32%. The gold distribution ratio in the slag phase increased from 5% to 20%, whereas that in the alloy phase decreased from 98% to 48%. Although most Ag was distributed in the alloy phase, the distribution ratio of Ag in the flue gas continued to increase with increasing Cl content in the system, reaching a maximum of 30%. Ag distributed in the slag phase was relatively stable, with a distribution ratio of 5%–10%. As the Cl content in the system increases, the distribution ratio of tin in the alloy phase decreases from 28% to 2%, whereas the tin content in the flue gas increases. At 1200 °C, the tin distribution ratio in the slag was approximately 50%–60%. When the reaction temperature was 1300 °C, Au was mainly enriched in the alloy and slag phases and changed less with the halogen content. When the Cl content in the system was 1 wt%, the distribution ratio of Ag in the alloy phase reached 98%, and an additional 2% of Ag entered the slag phase. As the Cl content in the system increased, the Ag content in the flue gas increased, with a distribution ratio of up to 10%. The presence of Cl significantly influenced the distribution behavior of Sn. As the Cl content in the system increased, the distribution ratio of tin in the alloy phase decreased from 20% to 2%, whereas that in the slag phase decreased from 60% to 36%. As the temperature increased, the distribution ratio of Au in the three terms showed a similar trend. However, the distribution behavior of Ag and Sn varies with temperature. When the Cl content in the system was 1 wt%, approximately 59% of Ag was enriched in the alloy phase, whereas 38% of Ag was distributed in the flue gas phase. When the Cl content in the system reached 5 wt%–10 wt%, the distribution ratio of Ag in the alloy phase increased to 80%, while Ag in the flue gas phase accounted for only 17%, and the silver content in the slag phase remained stable. Under high-temperature and Cl content conditions, Sn is prone to oxidation and volatilization, mainly distributed in slag and flue gas, whereas Sn in the alloy phase accounts for only approximately 1%.

Fig. 9 shows that gold and silver are mainly enriched in the alloy phase. When the equilibrium temperature was increased from 1200 °C to 1400 °C, the distribution ratio of Au in the slag increased from 2% to 30%. When the equilibrium temperature was 1300 °C, the distribution ratio of Ag in the alloy phase was greater than 85%. When the Br content in the system reached 10 wt%, the distribution ratio of Ag in the flue gas reached 13%. When the temperature was constant, as the Br content in the system increased, the

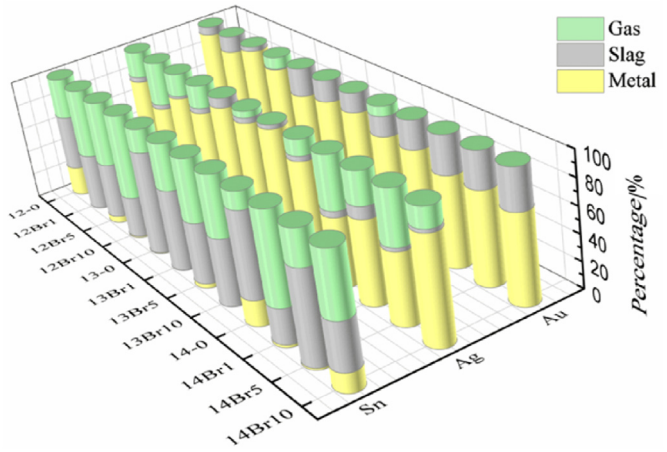

Fig. 9. Distribution behaviors of Au, Ag, and Sn in $CaBr_2$ adding system.

distribution ratio of Ag in the alloy phase increased, whereas the content in the slag and flue gas decreased. Br had a significant impact on the distribution behavior of Sn, and as the Br content in the system increased, the tin content in the alloy phase significantly decreased. When the Br content was constant, the distribution ratio of Sn in the alloy phase decreased with increasing temperature. At a constant temperature, the Sn content in the flue gas increased as the Br content increased, indicating that more Sn reacted with halogens and evaporated into the flue gas. Sn is a valuable metal, but its content in raw materials is low. These Sn that entered the metal and dust phases, could be recovered, and the criteria would be the leaching behavior of the dust and the refining process of the copper.

3.3. Mass balance and heat balance in pilot-scale practice

Electronic waste, low-grade copper scrap, industrial waste residue, SiO_2 flux, iron flux, and lump coal were added to the smelting furnace, and the ratio of e-waste was approximately 44.21%. There are various types of e-waste in the market. To obtain sufficient raw materials for industrial practice, e-waste materials from different resources were purchased, and the e-waste in the feeding was a mixture of crushed materials. Slurries purchased from the electroplating industry were used as starting materials and mainly comprised copper oxides and sulfates. Process air, oxygen, and natural gas were introduced for smelting, and the reaction temperature was controlled at approximately 1280 °C. Glass fiber, impurity metal oxides, and flux reacted to form slag. Rare and PMs such as copper, nickel, lead, gold, silver, platinum, and palladium formed a molten coarse copper phase, and the metal and slag phases were layered because of their different densities. Organic components such as plastics were burned and removed in the furnace and molten pool, resulting in a high-temperature flue gas. The smelting flue gas enters the secondary combustion chamber for combustion through the rising flue and is then recycled through a waste heat boiler. To prevent the regeneration of toxic substances such as dioxins, the flue gas from the boiler passes through a quenching tower and bag dust collection, and is then discharged after activated carbon adsorption, desulfurization, and denitrification treatment. This technology uses independently developed NRT technology to melt electronic waste and separate organic components. In addition, rare and PMs such as gold, silver, platinum, palladium, rhodium, selenium, and tellurium were enriched in crude copper, producing crude copper with a copper content of over 90 wt% (adjust the grade of crude copper based on the content of rare and PMs). The copper content in the water-quenched slag was less than 0.50 wt%, and the smelting dust and tail gas treatment tailings were used for further recovery of rare and PMs and valuable elements. The main process parameters for smelting process control are as follows: (1) mixed electronic waste treatment capacity: 5.95 t/h; (2) redox time: 3–5 h; (3) oxygen-enriched concentration: 21–40 vol%; (4) slag temperature: 1280 °C ± 50 °C; (4) process air volume: 10,000 $N \cdot m^3/h$; (5) air leakage rate: 1000 $N \cdot m^3/h$; (6) iron–silicon mass ratio: 0.9–1.4; (7) copper content in slag: less than 0.50 wt%. The heat balance of the melting process calculated using METSIM software is shown in Table 2.

Table 2 shows that the maximum heat revenue in the e-waste smelting process was the reaction enthalpy among starting materials, including metal oxidation and slagging reactions, which was 53,200 MJ/h, accounting for 66.94%, followed by the combustion heat of fuel, accounting for 33.04%. The total heat revenue of the entire smelting process is 794,765 MJ/h. In terms of heat expenditure, the smelting flue gas carries the highest heat item, reaching 38,445 MJ/h, accounting for 48.37% of the total heat expenditure, followed by the smelting slag, which carries the highest heat item, accounting for 28.47%. Using more e-waste may reduce the consumption of coal, but the heat balance of the system would be restored. According to the law of conservation of mass combined with actual production data, the NRT melting process was simulated and calculated using METSIM software, and the material balance obtained is shown in Table 3.

Table 3 shows that almost all copper, gold, and silver entered the copper phase during the smelting process of e-waste. The nickel was removed, but only a small amount of Ni entered the slag phase. Most of the tin entered the copper phase, with only a small amount entering the dust phase. Most lead and zinc volatilized into the dust, some entered the slag, and some entered the copper. Most chlorine and bromine entered the dust and gas phases. Compared with the dust of traditional smelting processes, the smelting dust generated during the e-waste treatment process contained several valuable metals with high contents. If the dust can be treated properly, the comprehensive recovery rates of copper, gold, silver, and tin can reach 99.10%, 99.99%, 99.63%, and 98.65%, respectively.

The co-smelting of e-waste with other traditional raw materials has the advantages of comprehensive recovery of treasures from

Table 2
The heat balance of on pilot e-waste smelting process.

Input	Energy (MJ/h)	Portion (%)	Output	Energy (MJ/h)	Portion (%)
Raw materials	16	0.02	Copper	4083	5.14
Fuel burning	26,260	33.04	Slag	22,625	28.47
Reaction enthalpy	53,200	66.94	Dust	1825	2.30
Total	79,476	100	Offgas	38,445	48.37
			Loss	12,498	15.72
			Total	79,476	100

Table 3
The mass balance of on pilot e-waste smelting process.

		Weight (t/h)	Cu		Fe		SiO_2		CaO		Al_2O_3	
			wt%	t/h	wt%	t/h	wt%	t/h	wt%	t/h	wt%	t/h
Input	E-waste	5.95	18.35	1.09	3.30	0.20	16.95	1.01	6.00	0.36	7.50	0.45
	Cu Scrap	0.80	92.00	0.74	3.00	0.02	0.00	0.00	0.00	0.00	0.00	0.00
	Slurry	4.46	14.95	0.67	23.11	1.03	15.01	0.67	9.66	0.43	1.59	0.07
	SiO_2	0.26	0.00	0.00	1.00	0.00	92.00	0.24	0.00	0.00	0.00	0.00
	CaO	0.64	0.00	0.00	0.00	0.00	4.50	0.03	50.07	0.32	0.00	0.00
	Coal	0.50	0.00	0.00	0.00	0.00	5.00	0.03	3.00	0.02	0.00	0.00
	Fe	0.85	0.00	0.00	65.00	0.55	0.00	0.00	0.00	0.00	0.00	0.00
Total		13.46		2.50		1.88		1.98		1.13		0.52
Output	Cu	2.39	95.32	2.28	0.15	0.00	0.00	0.00	0.00	0.00	0.00	0.00
	Slag	9.82	0.52	0.05	17.02	1.67	19.56	1.92	11.40	1.12	5.18	0.51
	Dust	1.23	13.60	0.17	17.19	0.21	4.88	0.06	0.87	0.01	0.91	0.01
	Offgas	0.02	0.00	0.00	0.00	0.00	0.00	0.00	0.00	0.00	0.00	0.00
Total		13.46		2.50		1.88		1.98		1.13		0.52

various materials and efficient utilization of chemical energy in organic components, both of which fit the scopes of circular economy and sustainable development. Knowledge of this process was established by studying the reaction mechanism and material balance.

4. Conclusions

In this study, the effect of halogen elements (F/Cl/Br) on the distribution behavior of Au, Ag, and Sn in the e-waste smelting process was investigated, and the $Cu–Fe_xO–SiO_2–CaO–Al_2O_3$ system was identified as the slag system. The energy and mass balance and element distribution behavior in one practical process were also investigated, and the following results were obtained.

(1) Optimized parameters for the e-waste smelting processes were; the slag temperature was 1280 °C, Fe/SiO_2 mass ratio was 0.62–0.95, CaO content was 15 wt%–20 wt%, and Al_2O_3 content was less than 20 wt%. The resulting crude copper contained more than 90 wt% copper, the slag contained approximately 0.5 wt% copper, and the recovery rate of copper, gold, and silver was greater than 98%.
(2) Au was mainly distributed in the alloy phase, and its behavior was closely related to the amount and temperature of halogen added. Ag was mainly enriched in the alloy phase, and a small amount of Ag entered the gas and slag phases. When calcium halide was added to the system, the proportion of Ag entering the gas phase increased. The amount of Ag entering the slag phase increased as the temperature increased. Sn was evenly distributed among the alloy, slag, and gas phases in the halogen-free systems. However, as the temperature increased or halides were added, more tin entered the slag and gas phases.
(3) Based on the practice of one e-waste smelting process, the mass and heat balance of the process were investigated using METSIM. The total heat revenue during the smelting process was 79,476 MJ/h, with the highest proportion of reaction heat from the furnace material, accounting for 66.94%, followed by fuel heat, accounting for 33.04% of the total. In the heat expenditure, the heat carried away by the smelting flue gas reached 38,445 MJ/h, accounting for 48.37% of the total heat expenditure, followed by the slag carrying the heat item, accounting for 28.47%. Almost all copper, gold, and silver enter the copper phase during the above e-waste smelting process.

Declaration of competing interest

The authors declare that they have no known competing financial interests or personal relationships that could have appeared to influence the work reported in this paper.

Acknowledgements

The research was financial supported by The science and technology innovation Program of Hunan Province, P.R. China (No. 2022RC1084).

References

Ahirwar, R., & Tripathi, A. K. (2021). E-waste management: A review of recycling process, environmental and occupational health hazards, and potential solutions. *Environmental Nanotechnology, Monitoring & Management, 15*, 100409.
Ashiq, A., Kulkarni, J., & Vithanage, M. (2019). Hydrometallurgical recovery of metals from E-waste. In M. Narasimha, V. Prasad, & M. Vithanage (Eds.), *Electronic waste management and treatment technology*. Oxford, UK: Butterworth-Heinemann.
Bazargan, A., Lam, K. F., & McKay, G. (2012). *Challenges and opportunities of E-waste management: Management, types, and challenge*. Hauppauge, New York, USA: Nova Science Publisher, Inc.
DOWA ECO-SYSTEM Co., Ltd. (2020). *Kosaka smelting and refining*. Available at: https://www.dowa-eco.co.jp/en/group/KSR.html. (Accessed 13 July 2023).
Dwivedy, M., & Mittal, R. K. (2010). Estimation of future outflows of e-waste in India. *Waste Management, 30*, 483–491.
Dwivedy, M., & Mittal, R. K. (2012). An investigation into e-waste flows in India. *Journal of Cleaner Production, 37*, 229–242.
Ebin, B., & Isik, M. I. (2016). Pyrometallurgical processes for the recovery of metals from WEEE. In A. Chagnes, G. Cote, C. Ekberg, et al. (Eds.), *WEEE recycling*. Amsterdam: Elsevier.
Hagelüken, C. (2006a). Recycling of electronic scrap at umicore precious metals refining. *Acta Metallurgica Slovaca, 12*, 111–120.
Hagelüken, C. (2006b). Recycling of electronic scrap at umicore's integrated metals smelter and refinery. *World of Metallurgy – ERZMETALL, 59*, 152–161.
Hoffmann, J. E. (1992). Recovering precious metals from electronic scrap. *Journal of Occupational Medicine, 44*, 43–48.
Innocenzi, V., De Michelis, I., & Vegliò, F. (2017). Design and construction of an industrial mobile plant for WEEE treatment: Investigation on the treatment of fluorescent powders and economic evaluation compared to other e-wastes. *Journal of the Taiwan Institute of Chemical Engineers, 80*, 769–778.
Işıldar, A. (2018). Biotechnologies for metal recovery from electronic waste and printed circuit boards. In F. Vegliò, & T. Birloaga (Eds.), *Waste electrical and electronic equipment recycling: Aqueous recovery methods*. Cambridge UK: Woodhead Publishing.
Kaya, M. (2016). Recovery of metals and nonmetals from electronic waste by physical and chemical recycling processes. *Waste Management, 57*, 64–90.
Khaliq, A., Rhamdhani, M., Brooks, G., & Masood, S. (2014). Metal extraction processes for electronic waste and existing industrial routes: A review and Australian perspective. *Resources, 3*, 152–179.
Kuehr, R. (2019). E-waste seen from a global perspective. In V. Goodship, A. Stevels, & J. Huisman (Eds.), *Waste electrical and electronic equipment (WEEE) handbook*. Amsterdam: Elsevier.

RCERGD. (2022). White paper on the recycling and comprehensive utilization of waste electrical and electronic products industry. In *Research center for electrical recycling and green development (RCERGD)*. Available at: https://www.doc88.com/p-63647037758847.html. (Accessed 13 July 2023) (in Chinese).

Song, X., Wang, J., Yang, J., & Lu, B. (2017). An updated review and conceptual model for optimizing WEEE management in China from a life cycle perspective. *Frontiers of Environmental Science & Engineering, 11*, 3.

Sum, E. Y. L. (1991). The recovery of metals from electronic scrap. *Journal of Occupational Medicine, 43*, 53–61.

Tunsu, C., & Retegan, T. (2016). Hydrometallurgical processes for the recovery of metals from WEEE. In A. Chagnes, G. Cote, C. Ekberg, et al. (Eds.), *WEEE recycling*. Amsterdam: Elsevier.